

# Deep Neural Network Driven Simulation Based Inference Method for Pole Position Estimation under Model Misspecification

Daniel Sadasivan,<sup>1,\*</sup> Isaac Cordero,<sup>1,†</sup> Andrew Graham,<sup>1,‡</sup> Cecilia Marsh,<sup>1,§</sup> Daniel Kupcho,<sup>1,¶</sup> Melana Mourad,<sup>1,\*\*</sup> and Maxim Mai<sup>2,3,††</sup>

<sup>1</sup>*Ave Maria University, Ave Maria, FL 34142, USA*

<sup>2</sup>*Albert Einstein Center for Fundamental Physics, Institute for Theoretical Physics, University of Bern, Sidlerstrasse 5, Bern, 3012, Switzerland*

<sup>3</sup>*Department of Physics, The George Washington University, 275 21st St, NW, Washington, 20052, District of Columbia, USA*

The method of Simulation Based Inference is shown to lead to a more accurate resonance parameter estimation than traditional  $\chi^2$  minimization in certain cases of model misspecification in a case-study of  $\pi\pi$  scattering and the  $\rho(770)$ -resonance. Models fit to certain data sets using  $\chi^2$  minimization can make inaccurate predictions for the pole position of the  $\rho(770)$ . SBI is shown to make more robust predictions for the pole position for the pole positions on these models and data sets. This is significant, both as a proof of concept that the SBI method can be used in cases of model misspecification, and because models of  $\pi\pi$  scattering are crucial part to many physical systems of contemporary interest ( $a_1(1260)$ ,  $\omega(782)$  etc.).

## I. INTRODUCTION

A traditional and widely-used method for parameter determination given data is to find the parameters that minimize  $\chi^2$  statistic. Simulation Based Inference (SBI) is an alternative method, developed and used in Refs. [1–4] and applied to a number of fields including particle physics [5], astrophysics [6, 7], the Mpemba Effect [8], neuroscience [9], climate science and evolutionary biology [10]. A pedagogical introduction in this matter can be found in Ref. [11]. In a nutshell, this method involves using a model to generate synthetic data, also referred to as pseudodata, and then using this pseudodata to construct a probability distribution for the model parameters given the data. The probability distribution is often modeled using deep neural networks.

Recent research has focused on understanding how SBI performs in cases in which either the data or the model is flawed, referred to as misspecification. Some works have shown challenges with the SBI method [12], some have used SBI as a method to test for model misspecification [13] while others develop version of SBI that are more robust to model misspecification [14, 15]. The present paper uses a version of SBI that is robust under model misspecification to predict parameters relevant to hadronic physics, first for a toy model and then for the actual data. It should be noted that in an ideal case in which (a) data are normally distributed around a model that is considered and (b) the minimization routine can find the global minimum,

the  $\chi^2$  method is guaranteed to give more probable fit parameters than the SBI method. However, in certain non-ideal cases, the SBI method might be able to outperform the method of  $\chi^2$  minimization. Thus, the aim of this paper is not to replace the standard practice of obtaining parameters through  $\chi^2$  minimization, but rather to introduce an alternative that can be useful in certain cases – specifically, in the presence of model misspecification.

The specific focus of this work are universal parameters of resonances, unstable particles that can be formed in scattering or decay processes. These parameters are encoded in the pole positions of the transition amplitudes. They are typically obtained by providing a suitable model for the latter respecting principles of S-matrix theory (possibly accommodating further symmetries), and fitting the model-parameters to the data. Then the amplitude (an analytic function of the complex-valued energy) is analytically continued to the unphysical Riemann sheets where poles are allowed, and are associated with resonances. For a pedagogical review see Ref. [16].

The vector, isovector  $\rho(770)$ -meson has quantum numbers that can overlap with those of a  $\pi\pi$  system. Thus, its parameters can be extracted from scattering data of two pions. Indeed, phase-shift data for this process are available [17, 18]. However, inconsistencies have been reported in the pole positions extracted from these data and the PDG values, obtained using data from a larger number of experiments, see e.g., Refs. [19–23]. An open question remains, thus, whether a method different from the  $\chi^2$ -minimization can be used to mitigate possible inconsistencies in the data extracting the pole positions of the  $\rho(770)$ . We note that the  $\rho(770)$ -resonance has also been studied in lattice QCD [24–36]. While beyond the scope of the current work, the connection of the SBI methodology to input from lattice QCD is not unthinkable, see, e.g., recent work [37] also

---

\* daniel.sadasivan@avemaria.edu  
† isaac.cordero@my.avemaria.edu  
‡ andrew.graham@my.avemaria.edu  
§ cecilia.marsh@my.avemaria.edu  
¶ daniel.kupcho@my.avemaria.edu  
\*\* melana.mourad@my.avemaria.edu  
†† maxim.mai@faculty.unibe.ch

building on alternative statistical tools.

The applications of this are not limited to the  $\rho(770)$ -resonance. Experimental data on  $K^-p \rightarrow K^-p$  and other final states in the low-energy regime is suffering under large ambiguities [38, 39] while also building a large bulk of an input required to access the universal parameters of the famous  $\Lambda(1405)$  two-pole structure [40]. Similarly, ambiguities in the meson-electroproduction data can lead to incorrect extraction of baryon resonance parameters [41]. Furthermore, models for  $\pi\pi$  scattering in the kinematic range covering the  $\rho(770)$ -resonance are also of large relevance for multi-hadron interaction. For example, understanding of the three-pion interaction requires the knowledge of the two-pion subsystem. For pertinent application ( $a_1(1260)$  and  $\omega(782)$ ) within the IVU approach [42] see Refs. [43–47] and for further related works Refs. [42, 48–65].

This work is not the first to apply methods involving neural networks to study resonance phenomena. Methods similar to SBI are used in: Ref. [66] to predict the type of a resonance; Ref. [67] to determine the pole position and pertinent Riemann sheets of the  $P_c(4312)^+$ ; Ref. [68] to predict the pole structure of  $P\psi N(4312)^+$ ; Ref. [69] to study the  $\Lambda(1405)$  resonance; Ref. [68] to obtain the scattering length and effective range of the  $X(3872)$  and the  $T_{cc}^+$ ; Ref. [70] to predict meson mass and width based only on their quantum numbers; Refs. [71, 72] to analyze hidden charm pentaquarks. Refs. [73–85] provide additional general methods applying neural networks or other machine learning methods to the study of pole positions or analytic continuation. What distinguishes the present paper from previous work in applying deep learning to the study of resonances is an explicit focus on making prediction in the case of model misspecification.

This paper is structured as follows. Section II A describes the specific method of SBI that is applied in this work. Section II B applies this method to a contrived example in which the correct answer is known to demonstrate the effectiveness of the method in comparison to  $\chi^2$  minimization. The method is then applied to  $\pi\pi$  scattering data. Section III A applies two separate models to two separate data sets isolating effects of each model and data set. Section III B uses an SBI method to determine what model to use with the data and then uses SBI to make a prediction for both data sets. Section IV discusses reasons why the SBI method might outperform the method of  $\chi^2$  minimization. The work is concluded in Sec. V.

## II. SIMULATION BASED INFERENCE APPLIED TO MODEL MISSPECIFICATION

### A. Methodology

This paper presents an alternative method for fitting a function, which can be written as  $f(x; \vec{a})$  with  $x$  and  $\vec{a}$

being an independent variable and model parameter list, respectively. The problem of fitting involves comparing this function to data to determine the most probable free-parameters. This is often done by minimizing a loss function such as the  $\chi^2$  statistic, which (if correlations in data are neglected) is given by

$$\chi^2 = \sum_i^{N_{data}} \frac{(f(x_i; \vec{a}) - y_i)^2}{\sigma_i^2}, \quad (1)$$

where  $x_i$  are independent measurements,  $y_i$  denote the dependent measurement with uncertainties  $\sigma_i$ . This well-known formula, can be used to find the most probable parameters,  $\vec{a}$  given the measured data  $y_i$  under the assumption that the data are normally distributed about the function for some values of  $\vec{a}$ , and the prior uniform probability distribution of fit parameters.

Under the case of model misspecification, meaning that no values of  $\vec{a}$  exist for which the data are normally distributed about the function, the most accurate parameters (given the data) may not be the parameters corresponding to the minimum  $\chi^2$ . SBI relies on different assumptions and therefore, in certain situations could give more accurate probability distributions in these situations. Because there are multiple ways that SBI can be implemented, we describe the method employed in this work below visualizing also the data pipeline in Fig. 1.

1. Sets of parameters  $\vec{a}_j$  are randomly generated. The range and probability distribution for this must be carefully chosen to minimize introduced bias. If most of the generated  $\vec{a}_j$  lead to a certain feature, the SBI method might predict this feature, whether or not the data contain evidence for this feature.
2. For each of these parameter sets, the function  $f$  is used to generate a set of pseudodata  $x^p$ ,  $y^p$  and  $\sigma^p$ , where  $x_i^p = x_i$  and  $\sigma_i^p = \sigma_i$  for provided independent variable and corresponding uncertainties. In other words, the independent variable and the uncertainty are the same for the pseudodata as for the actual data. The dependent variable is determined as  $y_i^p = R(f(x_i), \sigma_i)$ , i.e., a normally distributed random variable with a mean  $f(x_i)$  and standard deviation  $\sigma_i$ . In principle, this method can also be extended to assess the uncertainty on the dependent variable,  $x_i$ , as well. This can be of large relevance, e.g., for negative-strangeness meson-baryon systems [38, 86–93], where experimental data not only has large error bars on the measured cross sections but also on the energy variable. In these circumstances, pseudodata for the independent variable can be generated with  $x_i^p = R(x_i, \sigma_{x_i})$ , where  $\sigma_{x_i}$  is the uncertainty on  $x_i$ .
3. If necessary, only data points with the feature being studied are retained. For instance, in our example of  $\rho(770)$ -resonance, we only retain data points with physical poles in a realistic range. Clearly, this step can

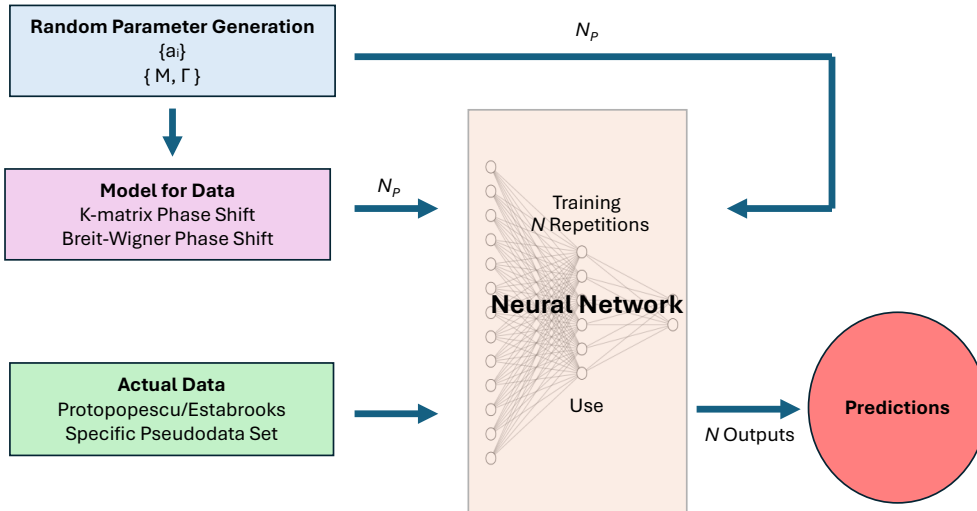


FIG. 1. A diagrammatic depiction of the data pipeline in the SBI method employed in this work. In each of the boxes on the left the middle/bottom row refer to the studied case of actual  $\pi\pi$  scattering data and the toy example, respectively.

introduce bias similar to the bias described in Step 1. For instance, if a neural network that is only trained on data corresponding to reasonable  $\rho$  poles returns a  $\rho$  pole that is no more accurate than the average of the training data, this is not evidence that the neural network has learned the data set. This will be discussed in detail in Sec. III C. The number of the remaining pseudodata sets is referred to in the following as  $N_P$ .

4. The pseudodata is used to train a neural network. The values  $y_i^p$  are used as the inputs of the neural network and the randomly generated  $\vec{a}$  used as outputs. A variety of loss functions could be used for this training, however, most commonly the mean squared error is used which is also employed in this work

5. Once the neural network is trained,  $y_i$  from the actual data are given as inputs and the outputs, predictions for  $\vec{a}$ , are recorded.

6. Steps 4. and 5. are repeated  $N$  times. This is necessary because there is some randomness in the selection of batches of  $\{y^p, \vec{a}\}$  while training the neural network. The output predictions for  $\vec{a}$  are stored.

7. The average values of the model parameter list obtained in the step 6 give the best fit predictions  $\bar{a}$ . Assuming a symmetric normal distribution of the values, the 95% confidence interval is obtained through standard deviation as  $\bar{a}_i \pm 1.96 \sigma(a_i) / \sqrt{N}$  for each model parameter  $a_i$ . Note that this confidence interval is for the average value of the  $\vec{a}$  outputs, which differs from the confidence interval for a single output. If the latter were the quantity of interest, the formula would not need the factor  $\sqrt{N}$ . Correlations between different parameters

can be extracted along the same lines.

## B. Toy Example

We begin with a toy example of a situation in which both SBI and  $\chi^2$  minimization are used for parameter estimation on a case designed to visualize why SBI might be more effective in cases of model misspecification.

Consider, a Breit-Wigner like parametrization of the scattering amplitude

$$T(E) = \frac{\sqrt{k}}{(E^2 - M^2) - iM\Gamma} \quad (2)$$

with a resonance mass  $M$ , width  $\Gamma$  and energy  $E$ . Using this parametrization, we generate pseudodata (unmodified data), i.e., phase-shift  $\delta(E) = \arctan(\text{Im} T(E)/\text{Re} T(E))$  that would be plausible if the parameters were given by  $M = 857 \text{ MeV}$  and  $\Gamma = 119 \text{ MeV}$  and then intentionally change the data (modified data) such that no values of  $M$  and  $\Gamma$  could plausibly have generated the data. Specifically, 11 unmodified points are generated for values of  $E$  ranging from 400 MeV to 1200 MeV in increments of 80 MeV, adding a normally-distributed random variable with a standard deviation of 0.05 to  $\delta(E)$ . After the unmodified data is calculated, the points are modified such that  $\delta(400) = 3.0$  and  $\delta(1200) = 0.2$  as depicted in Fig. 2. Note that this stark example is chosen as a first test contrasting  $\chi^2$  vs SBI methodology, only. Physically, more realistic case will be discussed in the later part of this article.

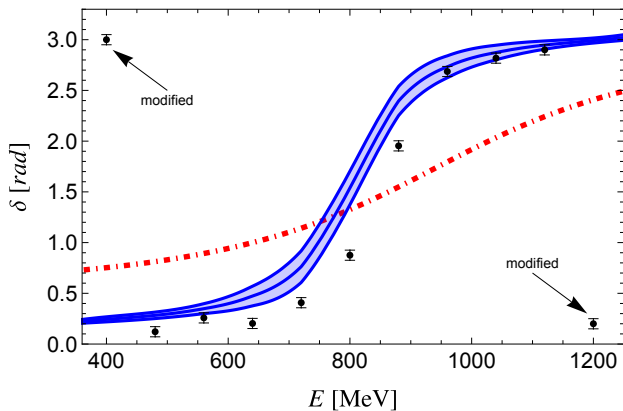


FIG. 2. Phase-shift data with endpoints that are intentionally modified to create a case of extreme model misspecification (black points) in comparison to the function that gives the minimum  $\chi^2$  (red dot-dashed) and the SBI result (connected blue lines including the pertinent confidence region in light blue). The SBI curve lies much closer to the unmodified data than the curve computed through  $\chi^2$  minimization.

The probability that the modified data could have been generated from any values of  $M$  and  $\Gamma$  is vanishingly small. The usual  $\chi^2$  minimization can, still, be applied to the modified data. The best fit returns values of  $M$  and  $\Gamma$  provided in Tab. I while the corresponding phase-shift is shown as the red dot-dashed curve in Fig. 2.

Simulation Based Inference is also employed, with its predictions shown the right column of Tab. I. There, we randomly generate  $N_P = 10^6$  points of training data with values of  $M$  uniformly distributed between 400 and 1200 and values of  $\Gamma$  uniformly distributed between 0 and 1000. The pseudodata is passed to a neural network. The details of this neural network are the same as the those of the neural networks employed elsewhere in this work (except the one used by the classifier network). Specifically, they include 4 hidden layers, with 40, 30, 20, and 10 nodes, respectively. Each node in each layer has a `relu` activation function. The output layer has two nodes with the leaky `relu` activation function. The mean squared error loss function is used. The neural networks are run for 1000 epochs or until they have been run for 20 epochs without improving the validation loss. In almost all cases, the latter occurs, indicating that further epochs would not improve the validation loss. The batch size chosen for the training process is 2000. The neural network is trained with the Adam

TABLE I. A comparison of the free parameters obtained through  $\chi^2$  minimization and SBI, using modified toy model data. The parameters generating the unmodified data are given in the second column.

	unmodified	$\chi^2$	SBI
$M$ [MeV]	857.0	887.3	799.3
$\Gamma$ [MeV]	119.0	662.6	136.9

optimizer. We note that the `relu` activation function, the Adam optimizer, and the mean squared error loss function are standard and have not been fine-tuned for a specific problem at hand. The leaky `relu` for the output layer was chosen because more common loss functions cannot return negative values. The number of nodes and layers was chosen somewhat arbitrarily, however, we have tried different numbers of nodes and layers and they give quite similar results, indicating that the exact number of nodes and layers does not alter the conclusion. We employ the same neural network architecture across all cases.

Taking a closer look on the results in Tab. I, we note that the SBI and  $\chi^2$  method give an  $M$  that is similarly close to the original  $M$  used to generate the unmodified data. At the same time, the value of  $\Gamma$  in the SBI method is closer by more than an order of magnitude than the value from the  $\chi^2$  method to the true value. The confidence region of  $\delta(E)$  predicted by SBI shown in the blue shaded area of Fig. 2. While this region does not cover all of the data points, it is much closer than the  $\delta(E)$  calculated with the parameters obtained through  $\chi^2$  minimization. This toy model demonstrates that, under model misspecification the SBI can outperform  $\chi^2$  minimization providing more accurate predictions of the underlying parameters.

In this toy example, the exact nature of the model misspecification is known. Thus, a reasonable alternative strategy could include, removing the visibly inaccurate data points as outliers or using different loss function, rather than the  $\chi^2$  function to reduce reliance on a few points. However, the strength of using SBI is that it did not have to identify why the data or model was flawed. In many cases of real application, the flaws that cause model misspecification are not identifiable. SBI can be used to obtain more accurate results even without identifying them.

### III. APPLICATION TO $\pi\pi$ SCATTERING AND THE $\rho(770)$

As discussed before, the properties of the  $\rho(770)$ -resonance can be accessed through  $\pi\pi$ -scattering data. As a representative example, we employ in this paper fits to the  $\pi\pi$ -scattering data using a K-matrix like approach reading

$$\begin{aligned}
 T(E) &= \tilde{v}(k_{\text{cm}}) \frac{1}{K_n^{-1}(E) - \Sigma(E)} \tilde{v}(k_{\text{cm}}), \\
 K_n^{-1}(E) &= M_\pi^2 \sum_{i=0}^{n-1} a_i \left( \frac{E^2}{M_\pi^2} \right)^i, \\
 \Sigma(E) &= \int_0^\infty dk k^2 \frac{1}{(2\pi)^3} \frac{1}{2E_k} \left( \frac{E^2}{4E_k^2} \right)^n \frac{\tilde{v}^2(k)}{\sigma - 4E_k^2 + i\epsilon}, \quad (3)
 \end{aligned}$$

TABLE II. The pole positions of the  $\rho(770)$  from SBI and  $\chi^2$  methods for data sets from Ref. [17] (Protopopescu) and Ref. [18] (Estabrooks). Two and three subtractions ( $n$ ) are used in both methods. Several reference values from the PDG [94] are provided in the lower table for comparison. All pole positions are visualized in Fig. 3.

Data	$n$	SBI				$\chi^2$				
		$a_0 \cdot 10^3$	$a_1 \cdot 10^3$	$a_2 \cdot 10^3$	$E^* [\text{MeV}]$	$a_0 \cdot 10^3$	$a_1 \cdot 10^3$	$a_2 \cdot 10^3$	$\chi_{\text{dof}}^2$	$E^* [\text{MeV}]$
Estabrooks	2	-444	+14.2		766.3(1.8) - $i$ 79.0(0.7)	-460	+15.6		12.8	750.3(0.6) - $i$ 69.8(0.5)
Protopopescu	2	-454	+14.9		763.7(1.0) - $i$ 75.5(0.3)	-467	+15.7		3.7	755.6(0.8) - $i$ 70.4(0.6)
Estabrooks	3	-188	-3.22	+0.41	772.8(2.9) - $i$ 73.9(0.6)	-223	+0.93	+0.39	3.6	766.8(1.5) - $i$ 74.0(0.7)
Protopopescu	3	-368	+8.90	+0.20	772.3(2.1) - $i$ 78.7(0.6)	-319	+6.30	+0.25	0.4	762.8(1.2) - $i$ 78.5(1.1)
All	3	-187	-3.17	+0.42	772.4(2.3) - $i$ 75.4(0.4)	-290	+4.10	+0.29	3.1	763.7(0.9) - $i$ 76.9(0.6)

Reference/PDG values

	$E^* = M - i\Gamma/2 [\text{MeV}]$
$e^+e^-$	775.3(0.3) - $i$ 73.9(0.5)
Photoproduction	769.0(1.0) - $i$ 75.9(1.3)
Other Reactions	769.0(0.9) - $i$ 75.5(0.9)

used, e.g., in Ref. [44]. Here,  $k_{\text{cm}} = \sqrt{E^2/4 + M_\pi^2}$ ,  $\tilde{v}(k) = \sqrt{16\pi/3k}$ ,  $E_k = \sqrt{k^2 + M_\pi^2}$ , while  $M_\pi$  denotes the pion mass. These models can use any number of subtractions ( $n$ ) which defines the number of free parameters of the model ( $a_i$ ). When the free parameters of these models (e.g.,  $n = 2$  or  $n = 3$  subtractions) are fit to the experimental data from Refs. [17] and [18] using  $\chi^2$  minimization the predicted pole positions differ significantly from the PDG values [94] including larger data sets. This problem is not unique to the K-matrix but was also discussed in a broader context [19–23] indicating the presence of certain inconsistencies in these data. This section covers the application of SBI to  $\pi\pi$  scattering to make predictions for the pole position of the  $\rho(770)$ . This is done for each data set and model separately in Sec. III A and all together in Sec. III B.

### A. Predictions for Individual Data Sets and Models

In this section, we apply two and three subtraction models (c.f.  $n$  in Eq. (3)) to data from Refs. [17] or [18] to which we refer to as Protopopescu data and Estabrooks data after the respective first author of each publication. This defines four different cases, allowing us to assess the effects that might be specific to one model/data set.

The best fit parameters with  $\chi^2$  minimization are determined and shown including the extracted pole positions in the right part of the Tab. II. Left part of the same table collects the results of the corresponding SBI method. Everywhere, the uncertainties are calculated with bootstrap resampling, while the pseudodata are generated following the method described in Sec. II A with some details relegated to Sec. III C. The bottom of Tab. II gives the reference values taken from the PDG tables [94] where larger range of data sets and factors

were used. We emphasize that our goal here is not to improve on theoretical tools (see, e.g., Refs. [20, 95–97]) but rather to study possible alternatives to the usually employed  $\chi^2$  methodology. The positions for each case for both the  $\chi^2$  method and the SBI method, as well as the PDG pole positions are visualized in Fig. 3.

In all four cases, the SBI pole position is closer to the pole position from the most precisely determined  $e^+e^-$  data. In three of the four cases, the SBI is closer to all predictions of the data than the PDG. In the Estabrooks  $n = 3$  case, the  $\chi^2$  central predicted value is slightly closer to the photoproduction data and data from other reactions. However, the SBI prediction is fewer standard deviations away from these data than the  $\chi^2$  predictions. Furthermore, the one-standard-deviation confidence region for the SBI prediction in this case overlaps with the equivalent confidence regions for all three PDG reference values. This indicates that being closer to the PDG values for the photoproduction data and other data might not even be a sign of greater accuracy. Overall, it is reasonable to claim that in all four cases, the SBI method leads to pole predictions that are as close or closer to the reference values than the method of  $\chi^2$  minimization.

### B. Combined Fit and Classifier Network

In this section, we discuss how to incorporate information for all four cases. The two data sets can be combined into a single data set, but both different models cannot be combined – one or another must be chosen. The method we use to determine the best model to use to fit the data is similar to the SBI method used in this work, see Sec. II A. A large number of pseudodata sets are generated from models with various number

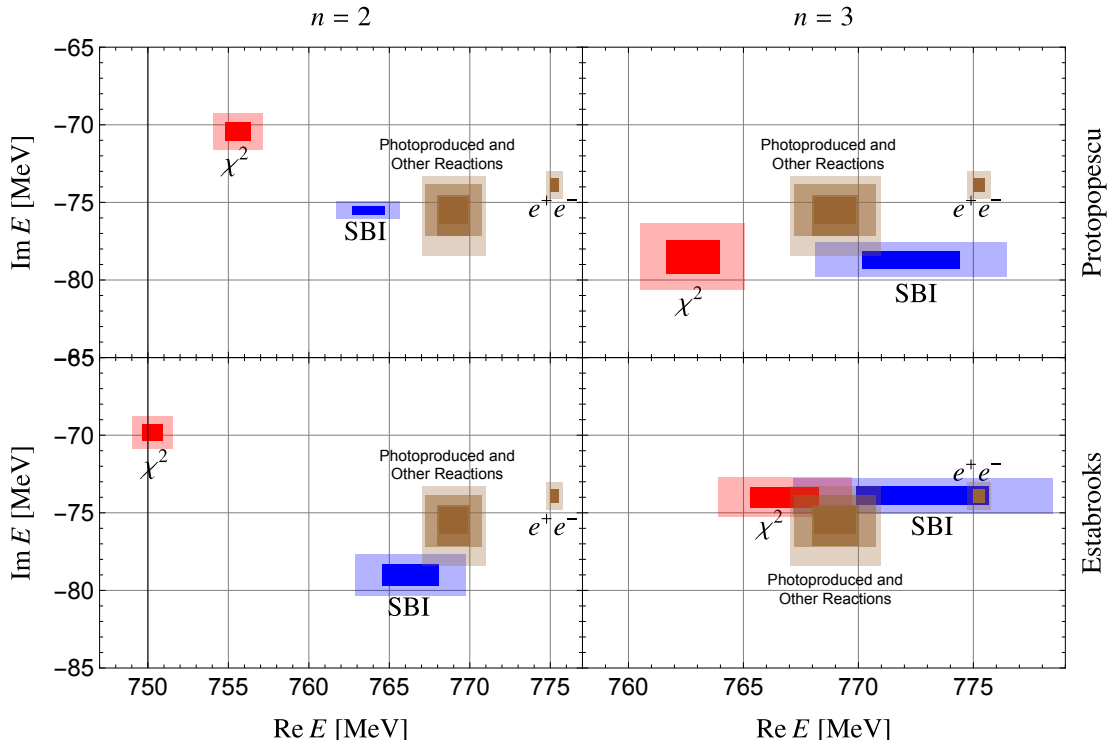


FIG. 3. The pole position confidence regions of the  $\rho(770)$  for data sets from Ref. [17] (Protopopescu) and [18] (Estabrooks), using two and three subtractions. The red rectangles (1- and 2-standard deviations) give the confidence region obtained through  $\chi^2$  minimization and the blue that of the SBI. The brown rectangles give the PDG values for various types of experiments which serve as a benchmark. In all cases, the SBI method makes predictions for the  $\rho$ -pole that as close or closer to the reference values than the  $\chi^2$  method.

of subtractions (c.f.,  $n$  in Eq. (3)). Only pseudodata points that have realistic pole positions are retained as discussed in Sec. III C. A neural network is then trained to predict the number of subtractions that generated the pseudodata. Finally, the experimental data is given to the neural network returning an estimate of the probability that this data was generated from a given model assuming it was generated from such model types. This classifier neural network uses the softmax activation function for the final node. The network is trained using a cross-entropy loss function. The estimated probabilities  $P(n)$  with uncertainties in the parenthesis read

$$\begin{aligned}
 P(1) &= 0.00067(00003), \\
 P(2) &= 0.06482(00095), \\
 P(3) &= 0.86657(00122), \\
 P(4) &= 0.06791(01004), \\
 P(5) &= 0.00001(00000).
 \end{aligned}
 \tag{4}$$

These results indicate that, if the actual data were generated from a K-matrix model, three subtractions is most likely to have generated it, which we use in the what follows.

The SBI predictions using both data sets are given in bottom row of Tab. II together with the  $\chi^2$  parameters, while the predicted pole positions are also depicted in the left panel of Fig. 4. Right panel of Fig. 4 shows the model

phase-shift predictions in comparison to the data. The minimum  $\chi^2$  per degree of freedom is 3.1 (see Tab. II). This indicates that – just as with the data in the toy example – the probability these points could have been generated from this model is negligible. While the same holds for the SBI, it is also apparent that it provides predictions (left panel of Fig. 4) which are much closer to the reference values than those of the  $\chi^2$  method. This indicates that possible ambiguities in the data are systematically better handled in the SBI method.

### C. Training Data Generation and Tests for Bias

We generate pseudodata as described in Step 1 in Sec. II A. The parameters  $a_0$ ,  $a_1$ ,  $a_2$  are generated randomly with a uniform distribution within the following ranges  $[-\text{GeV}^2/M_\pi^2, \text{GeV}^2/M_\pi^2]$ ,  $[-1, 1]$ ,  $[-M_\pi^2/\text{GeV}^2, M_\pi^2/\text{GeV}^2]$ , respectively. These ranges are well beyond the values that would generate reasonable  $\rho(770)$ -resonance poles.

Next, as described in Step 3 of Sec. II A, we include only parameters which lead to a pole position within the largest possible square centered on the pole-position (obtained from the  $\chi^2$  method) that is below the real axis. In other words, if the  $\chi^2$  determined pole from the actual data has a position  $E^* = a - ib$ , we retain

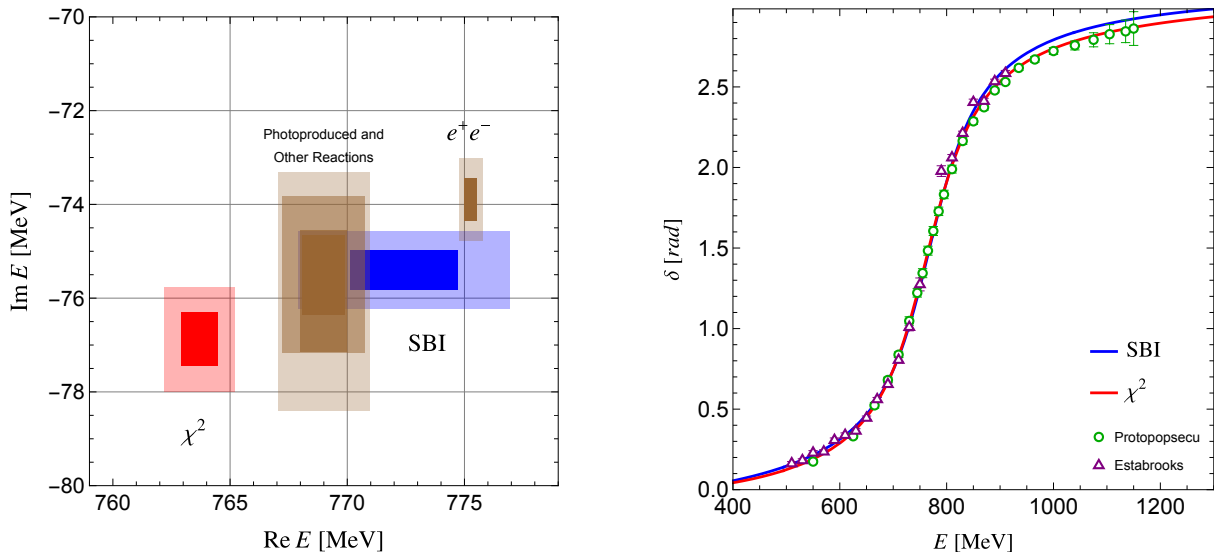


FIG. 4. Left: A comparison of the SBI method (blue) and the  $\chi^2$  method (red) for the pole positions. The SBI pole position is closer to all PDG data sets than the  $\chi^2$  minimization. Right: A comparison of the phase-shifts for the SBI method and the  $\chi^2$  method with the Protopopsecu [17] and Estabrooks [18] data. The best fit  $\chi^2_{\text{dof}}$  value and further details can be found in Tab. II.

pseudodata points if the corresponding  $\chi^2$  determined pole  $E_P^* = x - iy$  fulfills  $a - b < x < a + b$  and  $2b < y < 0$ . Such a method centers the range of allowed pole positions on the  $E^*$  but does not require addition choices of ranges. This pseudodata is generated until  $N_P = 10^6$  points of training data are obtained. This step is necessary because most randomly generated parameters do not lead to any physical pole and only approximately 2% lead to a pole in the range in which we retain data. If this step were not performed, the neural network with the lowest loss function would be one that made the best predictions on the majority of the training data, which did not have poles. We emphasize again that the goal of this work is not to provide a universal neural network trained to assess any scenario but rather to provide an alternative method (SBI) to the usual  $\chi^2$  minimization for extracting pole positions from data which includes ambiguities.

The training data is given to a neural network with exactly the same details as the neural network used in the toy example of Sec. II B. For each case, the neural networks are run  $N = 100$  times. Randomness in optimization such as the batch selection leads to different final results. These  $N = 100$  different results are used to calculate the uncertainty as described in Step 7. in Sec. II A.

A common concern to many applications of neural networks and AI in general is that a possible bias or prior in the pseudodata might lead to unnaturally accurate results. For example, even though the range of values in which the poles are retained is centered around the  $\chi^2$  pole, it is possible that the pole values for randomly generated parameters that fall in this range tend to be clustered closer to the reference PDG results. To address this, we calculate the pole positions for each

point of the training data ( $10^6$ ) and take the average as provided in Tab. III. These positions can also be compared to the pole positions obtained previously for the two methods in Tab. II. Quantitatively, this is encoded in the provided distances in Tab. III between the poles from the two methods and the average training data poles for each model and data set. For  $n = 3$  and all data combinations, the average of the poles from the training data is quite far from the predictions of either method. The distance to either method is more than three times as large as the that between the methods themselves. This demonstrates that the particular choice of the training data cannot have been the reason for the better performance of the SBI method. For the  $n = 2$  cases, the average of the training data pole positions is closer to SBI result. This indicates that the data used to train the neural network might slightly influence the accuracy of the SBI method. However, the fact that the average training data pole is roughly equidistant from the predictions from the two methods in both cases indicates that this bias is not the primary cause of the success of the SBI method. Furthermore, we note that the distance from the SBI result to the reference values is much smaller than that to the training data, or between the  $\chi^2$  result to the reference values as well, see Fig. 3.

#### IV. DISCUSSION

In the previous sections we have demonstrated that SBI can be more accurate than  $\chi^2$  minimization in certain cases of model misspecification. In this section, we discuss what causes this result. To some extent, we

TABLE III. The average of the pole position calculated from each point in the pseudodata used to train the neural network. The right three columns give the distance in MeV between the pole positions in this table and the pole positions predicted by the SBI method and  $\chi^2$  minimization method in Tab. II.

Data	$n$	pseudodata $E^*$ [MeV]	Distance $\chi^2$ to pseudodata	Distance pseudodata to SBI	Distance SBI to $\chi^2$
Estabrooks	2	$757.4 - i 80.8$	13.2	9.1	18.5
Protopopescu	2	$757.3 - i 81.0$	10.6	8.3	9.5
Estabrooks	3	$766.7 - i 45.0$	29.0	29.5	6.0
Protopopescu	3	$764.8 - i 44.4$	34.2	35.1	9.5
All	3	$766.1 - i 44.1$	32.9	32.3	8.8

are limited to speculation, because, in general neural networks are "black boxes" which behavior cannot be easily inferred from the details of the network [98]. Still, we can speak more certainly about which information the neural network has access to that the  $\chi^2$  method does not.

Most importantly, the SBI method seems to contain information about the shape of the curve. For instance, in the case of the toy example in Fig. 2, the two modified data points do not follow the shape of any possible phase-shift curve but the 9 unmodified points do. On the other hand, the  $\chi^2$  method does not contain information about the shape of the curve; as long as the curve comes close to the data points, quantities such as the curvature or slope do not influence the result. The case of the SBI applied to the  $\rho(770)$  is not quite as simple because the data points cannot be divided into points that are close to a possible phase-shift curve and points that are not. However, in this case as well, the SBI method can make use of additional information about the shape of the curve.

Thus, it is quite plausible, although not certain, that this information might be responsible for the greater accuracy of the SBI methods in the situations that have been considered. Certain is that the SBI method provides significantly different (and lies closer to reference values which include larger data sets) results than the  $\chi^2$  minimization method.

## V. CONCLUSION

We have presented a method of Simulation Based Inference and shown it to be a viable alternative method to the  $\chi^2$  minimization in case of model misspecification both for a toy example and for the case of the actual  $\pi\pi$  phase-shift data used to predict the  $\rho(770)$ -resonance parameter. In the latter case, the SBI, indeed provides

resonance parameters closer to the reference values for two different models and two different data sets indicating the robustness of the method. Additionally, a classifier neural network was employed to determine which model is most likely to have generated both sets of data simultaneously. SBI was then employed to determine the best parameters for this model. These parameters can be applied, beyond determination of the  $\rho(770)$  to study of three-body states such as the  $a_1(1260)$ .

While it is difficult to exactly determine the reason why the SBI method outperforms the  $\chi^2$  minimization method in the described cases of model misspecification, we have speculated that the effectiveness of the SBI is due to the additional information the method has access to. Specifically, it can make use of the general shapes of the function and a knowledge of the functions of all possible parameters.

The SBI cannot outperform  $\chi^2$  minimization in cases that are close to ideal, and for this reason, we do not believe that it will replace the latter method. However, the strength of the method presented here gives strong reason to believe that application to other situations where data (including possible ambiguities) can lead to model misspecification would allow for a more robust determination of pole parameters.

## ACKNOWLEDGMENTS

We are grateful to Saverio Perugini, Alex Tsai, Dave Ireland and Anastasios Belias for useful discussions regarding machine learning applications. We thank Michael Döring for helping in developing useful algorithms used in parts of this work. The work of MM was funded through the Heisenberg Programme by the Deutsche Forschungsgemeinschaft (DFG, German Research Foundation) – 532635001.

[1] Simon Tavaré, David J Balding, Robert C Griffiths, and Peter Donnelly, "Inferring coalescence times from DNA sequence data," *Genetics* **145**, 505–518 (1997).

[2] Donald B Rubin, "Bayesianly justifiable and relevant frequency calculations for the applied statistician," *The Annals of Statistics* **12**, 1151–1172 (1984).

- [3] Peter J Diggle and Richard J Gratton, “Monte Carlo methods of inference for implicit statistical models,” *Journal of the Royal Statistical Society: Series B (Methodological)* **46**, 193–212 (1984).
- [4] Mark A Beaumont, Wenyang Zhang, and David J Balding, “Approximate Bayesian computation in population genetics,” *Genetics* **162**, 2025–2035 (2002).
- [5] Johann Brehmer and Kyle Cranmer, “Simulation-based inference methods for particle physics,” (2020), [arXiv:2010.06439 \[hep-ph\]](#).
- [6] Siddharth Mishra-Sharma, “Inferring dark matter substructure with astrometric lensing beyond the power spectrum,” *Mach. Learn. Sci. Tech.* **3**, 01LT03 (2022), [arXiv:2110.01620 \[astro-ph.CO\]](#).
- [7] Ronan Legin, Yashar Hezaveh, Laurence Perreault Levasseur, and Benjamin Wandelt, “Simulation-Based Inference of Strong Gravitational Lensing Parameters,” (2021), [arXiv:2112.05278 \[astro-ph.CO\]](#).
- [8] Felipe Amorim, Joey Wisely, Nathan Buckley, Christiana DiNardo, and Daniel Sadasivan, “Predicting the mpemba effect using machine learning,” *Physical Review E* **108** (2023), [10.1103/physreve.108.024137](#).
- [9] Pedro J Gonçalves, Jan-Matthis Lueckmann, Michael Deistler, Marcel Nonnenmacher, Kaan Öcal, Giacomo Bassetto, Chaitanya Chintaluri, William F Podlaski, Sara A Haddad, Tim P Vogels, David S Greenberg, and Jakob H Macke, “Training deep neural density estimators to identify mechanistic models of neural dynamics,” *eLife* **9**, e56261 (2020).
- [10] Grace AVECILLA, Julie Chuong, Fangfei Li, Gavin Sherlock, David Gresham, and Yoav Ram, “Simulation-based inference of evolutionary parameters from adaptation dynamics using neural networks,” (2021).
- [11] Astro Automata, “A tutorial on simulation-based inference,” (2020), accessed: 2025-05-23.
- [12] Patrick Cannon, Daniel Ward, and Sebastian M. Schmon, “Investigating the impact of model misspecification in neural simulation-based inference,” (2022), [arXiv:2209.01845 \[stat.ML\]](#).
- [13] Noemi Anau Montel, James Alvey, and Christoph Weniger, “Tests for model misspecification in simulation-based inference: From local distortions to global model checks,” *Phys. Rev. D* **111**, 083013 (2025), [arXiv:2412.15100 \[astro-ph.IM\]](#).
- [14] Daolang Huang, Ayush Bharti, Amauri Souza, Luigi Acerbi, and Samuel Kaski, “Learning robust statistics for simulation-based inference under model misspecification,” (2023), [arXiv:2305.15871 \[stat.ML\]](#).
- [15] Antoine Wehenkel, Juan L. Gamella, Ozan Sener, Jens Behrmann, Guillermo Sapiro, Marco Cuturi, and Jörn-Henrik Jacobsen, “Addressing misspecification in simulation-based inference through data-driven calibration,” (2024), [arXiv:2405.08719 \[stat.ML\]](#).
- [16] Maxim Mai, “Theory of resonances,” (2025), [arXiv:2502.02654 \[hep-ph\]](#).
- [17] S. D. Protopopescu, M. Alston-Garnjost, A. Barbaro-Galtieri, Stanley M. Flatte, J. H. Friedman, T. A. Lasinski, G. R. Lynch, M. S. Rabin, and F. T. Solmitz, “ $\pi\pi$  Partial Wave Analysis from Reactions  $\pi^+p \rightarrow \pi^+\pi^-\Delta^{++}$  and  $\pi^+p \rightarrow K^+K^-\Delta^{++}$  at 7.1-GeV/c,” *Phys. Rev. D* **7**, 1279 (1973).
- [18] P. Estabrooks and Alan D. Martin, “ $\pi\pi$  Phase Shift Analysis Below the  $K\bar{K}$  Threshold,” *Nucl. Phys.* **B79**, 301–316 (1974).
- [19] B. Ananthanarayan, G. Colangelo, J. Gasser, and H. Leutwyler, “Roy equation analysis of  $\pi\pi$  scattering,” *Phys. Rept.* **353**, 207–279 (2001), [arXiv:hep-ph/0005297 \[hep-ph\]](#).
- [20] G. Colangelo, J. Gasser, and H. Leutwyler, “ $\pi\pi$  scattering,” *Nucl. Phys.* **B603**, 125–179 (2001), [arXiv:hep-ph/0103088 \[hep-ph\]](#).
- [21] R. Garcia-Martin, R. Kaminski, J. R. Pelaez, J. Ruiz de Elvira, and F. J. Yndurain, “The Pion-pion scattering amplitude. IV: Improved analysis with once subtracted Roy-like equations up to 1100 MeV,” *Phys. Rev. D* **83**, 074004 (2011), [arXiv:1102.2183 \[hep-ph\]](#).
- [22] Gilberto Colangelo, Martin Hoferichter, and Peter Stoffer, “Two-pion contribution to hadronic vacuum polarization,” *JHEP* **02**, 006 (2019), [arXiv:1810.00007 \[hep-ph\]](#).
- [23] J. R. Pelaez, A. Rodas, and J. Ruiz De Elvira, “Global parameterization of  $\pi\pi$  scattering up to 2 GeV,” *Eur. Phys. J. C* **79**, 1008 (2019), [arXiv:1907.13162 \[hep-ph\]](#).
- [24] S. Aoki *et al.* (CS), “ $\rho$  Meson Decay in 2+1 Flavor Lattice QCD,” *Phys. Rev. D* **84**, 094505 (2011), [arXiv:1106.5365 \[hep-lat\]](#).
- [25] Jozef J. Dudek, Robert G. Edwards, and Christopher E. Thomas (Hadron Spectrum), “Energy dependence of the  $\rho$  resonance in  $\pi\pi$  elastic scattering from lattice QCD,” *Phys. Rev. D* **87**, 034505 (2013), [Erratum: *Phys. Rev. D* **90**, 099902 (2014)], [arXiv:1212.0830 \[hep-ph\]](#).
- [26] Gunnar S. Bali, Sara Collins, Antonio Cox, Gordon Donald, Meinulf Göckeler, C. B. Lang, and Andreas Schäfer (RQCD), “ $\rho$  and  $K^*$  resonances on the lattice at nearly physical quark masses and  $N_f = 2$ ,” *Phys. Rev. D* **93**, 054509 (2016), [arXiv:1512.08678 \[hep-lat\]](#).
- [27] David J. Wilson, Raul A. Briceño, Jozef J. Dudek, Robert G. Edwards, and Christopher E. Thomas, “Coupled  $\pi\pi, K\bar{K}$  scattering in  $P$ -wave and the  $\rho$  resonance from lattice QCD,” *Phys. Rev. D* **92**, 094502 (2015), [arXiv:1507.02599 \[hep-ph\]](#).
- [28] Ziwen Fu and Lingyun Wang, “Studying the  $\rho$  resonance parameters with staggered fermions,” *Phys. Rev. D* **94**, 034505 (2016), [arXiv:1608.07478 \[hep-lat\]](#).
- [29] Constantia Alexandrou, Luka Leskovec, Stefan Meinel, John Negele, Srijit Paul, Marcus Petschlies, Andrew Pochinsky, Gumaro Rendon, and Sergey Syritsyn, “ $P$ -wave  $\pi\pi$  scattering and the  $\rho$  resonance from lattice QCD,” *Phys. Rev. D* **96**, 034525 (2017), [arXiv:1704.05439 \[hep-lat\]](#).
- [30] Christian Andersen, John Bulava, Ben Hörz, and Colin Morningstar, “The  $I = 1$  pion-pion scattering amplitude and timelike pion form factor from  $N_f = 2 + 1$  lattice QCD,” *Nucl. Phys. B* **939**, 145–173 (2019), [arXiv:1808.05007 \[hep-lat\]](#).
- [31] Markus Werner *et al.* (Extended Twisted Mass), “Hadron-Hadron Interactions from  $N_f = 2 + 1 + 1$  Lattice QCD: The  $\rho$ -resonance,” *Eur. Phys. J. A* **56**, 61 (2020), [arXiv:1907.01237 \[hep-lat\]](#).
- [32] Dehua Guo, Andrei Alexandru, Raquel Molina, Maxim Mai, and Michael Döring, “Extraction of isoscalar  $\pi\pi$  phase-shifts from lattice QCD,” *Phys. Rev. D* **98**, 014507 (2018), [arXiv:1803.02897 \[hep-lat\]](#).
- [33] B. Hu, R. Molina, M. Döring, M. Mai, and A. Alexandru, “Chiral extrapolations of the  $\rho(770)$  meson in  $N_f = 2 + 1$  lattice QCD simulations,” *Phys. Rev. D* **96**, 034520 (2017), [arXiv:1704.06248 \[hep-lat\]](#).

- [34] Bin Hu, Raquel Molina, Michael Doring, Andrei Alexandru, and Dehua Guo, “Two-flavor simulations of the  $\rho(770)$  and the role of the  $K\bar{K}$  channel,” *PoS LATTICE2016*, 096 (2016).
- [35] Dehua Guo, Andrei Alexandru, Raquel Molina, and Michael Döring, “Rho resonance parameters from lattice QCD,” *Phys. Rev. D* **94**, 034501 (2016), [arXiv:1605.03993 \[hep-lat\]](#).
- [36] Matthias Fischer, Bartosz Kostrzewa, Maxim Mai, Marcus Petschlies, Ferenc Pittler, Martin Ueding, Carsten Urbach, and Markus Werner (Extended Twisted Mass, ETM), “The  $\rho$ -resonance from Nf=2 lattice QCD including the physical pion mass,” *Phys. Lett. B* **819**, 136449 (2021), [arXiv:2006.13805 \[hep-lat\]](#).
- [37] Miguel Salg, Fernando Romero-López, and William I. Jay, “Bayesian Analysis and Analytic Continuation of Scattering Amplitudes from Lattice QCD,” (2025), [arXiv:2506.16161 \[hep-lat\]](#).
- [38] D. Sadasivan, M. Mai, and M. Döring, “S- and p-wave structure of  $S = -1$  meson-baryon scattering in the resonance region,” *Phys. Lett. B* **789**, 329–335 (2019), [arXiv:1805.04534 \[nucl-th\]](#).
- [39] Ferenc Pittler, Maxim Mai, Ulf-G. Meißner, Ryan F. Ferguson, Peter Hurck, David G. Ireland, and Bryan McKinnon, “Universal parameters of the  $\Lambda(1380)$ , the  $\Lambda(1405)$  and their isospin partners from a combined analysis of Lattice QCD and experimental results,” (2025), [arXiv:2507.14283 \[hep-ph\]](#).
- [40] Maxim Mai, “Review of the  $\Lambda(1405)$  A curious case of a strangeness resonance,” *Eur. Phys. J. ST* **230**, 1593–1607 (2021), [arXiv:2010.00056 \[nucl-th\]](#).
- [41] Maxim Mai, Michael Döring, Carlos Granados, Helmut Haberzettl, Ulf-G. Meißner, Deborah Rönchen, Igor Strakovsky, and Ron Workman (Jülich-Bonn-Washington), “Jülich-Bonn-Washington model for pion electroproduction multipoles,” *Phys. Rev. C* **103**, 065204 (2021), [arXiv:2104.07312 \[nucl-th\]](#).
- [42] M. Mai, B. Hu, M. Doring, A. Pilloni, and A. Szczepaniak, “Three-body Unitarity with Isobars Revisited,” *Eur. Phys. J. A* **53**, 177 (2017), [arXiv:1706.06118 \[nucl-th\]](#).
- [43] D. Sadasivan, M. Mai, H. Akdag, and M. Döring, “Dalitz plots and lineshape of  $a_1(1260)$  from a relativistic three-body unitary approach,” *Phys. Rev. D* **101**, 094018 (2020), [Erratum: *Phys.Rev.D* 103, 019901 (2021)], [arXiv:2002.12431 \[nucl-th\]](#).
- [44] Daniel Sadasivan, Andrei Alexandru, Hakan Akdag, Felipe Amorim, Ruairí Brett, Chris Culver, Michael Döring, Frank X. Lee, and Maxim Mai, “Pole position of the  $a_1(1260)$  resonance in a three-body unitary framework,” *Phys. Rev. D* **105**, 054020 (2022), [arXiv:2112.03355 \[hep-ph\]](#).
- [45] Maxim Mai, Andrei Alexandru, Ruairí Brett, Chris Culver, Michael Döring, Frank X. Lee, and Daniel Sadasivan (GWQCD), “Three-Body Dynamics of the  $a_1(1260)$  Resonance from Lattice QCD,” *Phys. Rev. Lett.* **127**, 222001 (2021), [arXiv:2107.03973 \[hep-lat\]](#).
- [46] Yuchuan Feng, Fernando Gil, Michael Döring, Raquel Molina, Maxim Mai, Vanamali Shastry, and Adam Szczepaniak, “A unitary coupled-channel three-body amplitude with pions and kaons,” *Phys. Rev. D* **110**, 094002 (2024), [arXiv:2407.08721 \[nucl-th\]](#).
- [47] Haobo Yan, Maxim Mai, Marco Garofalo, Ulf-G. Meißner, Chuan Liu, Liuming Liu, and Carsten Urbach, “ $\omega$  Meson from Lattice QCD,” *Phys. Rev. Lett.* **133**, 211906 (2024), [arXiv:2407.16659 \[hep-lat\]](#).
- [48] Michael Döring, Johann Haidenbauer, Maxim Mai, and Toru Sato, “Dynamical coupled-channel models for hadron dynamics,” (2025), [arXiv:2505.02745 \[nucl-th\]](#).
- [49] Marco Garofalo, Maxim Mai, Fernando Romero-López, Akaki Rusetsky, and Carsten Urbach, “Three-body resonances in the  $\varphi^4$  theory,” *JHEP* **02**, 252 (2023), [arXiv:2211.05605 \[hep-lat\]](#).
- [50] Maxim Mai, Michael Döring, and Akaki Rusetsky, “Multi-particle systems on the lattice and chiral extrapolations: a brief review,” *Eur. Phys. J. ST* **230**, 1623–1643 (2021), [arXiv:2103.00577 \[hep-lat\]](#).
- [51] Andrei Alexandru, Ruairí Brett, Chris Culver, Michael Döring, Dehua Guo, Frank X. Lee, and Maxim Mai, “Finite-volume energy spectrum of the  $K^-K^-K^-$  system,” *Phys. Rev. D* **102**, 114523 (2020), [arXiv:2009.12358 \[hep-lat\]](#).
- [52] Chris Culver, Maxim Mai, Ruairí Brett, Andrei Alexandru, and Michael Döring, “Three pion spectrum in the  $I = 3$  channel from lattice QCD,” *Phys. Rev. D* **101**, 114507 (2020), [arXiv:1911.09047 \[hep-lat\]](#).
- [53] M. Mai, M. Döring, C. Culver, and A. Alexandru, “Three-body unitarity versus finite-volume  $\pi^+\pi^+\pi^+$  spectrum from lattice QCD,” *Phys. Rev. D* **101**, 054510 (2020), [arXiv:1909.05749 \[hep-lat\]](#).
- [54] Maxim Mai, Chris Culver, Andrei Alexandru, Michael Döring, and Frank X. Lee, “Cross-channel study of pion scattering from lattice QCD,” *Phys. Rev. D* **100**, 114514 (2019), [arXiv:1908.01847 \[hep-lat\]](#).
- [55] C. Culver, M. Mai, A. Alexandru, M. Döring, and F. X. Lee, “Pion scattering in the isospin  $I = 2$  channel from elongated lattices,” *Phys. Rev. D* **100**, 034509 (2019), [arXiv:1905.10202 \[hep-lat\]](#).
- [56] Maxim Mai, “3-body quantization condition in unitary isobar formalism,” *PoS LATTICE2018*, 050 (2018), [arXiv:1810.00604 \[hep-lat\]](#).
- [57] Maxim Mai and Michael Doring, “Finite-Volume Spectrum of  $\pi^+\pi^+$  and  $\pi^+\pi^+\pi^+$  Systems,” *Phys. Rev. Lett.* **122**, 062503 (2019), [arXiv:1807.04746 \[hep-lat\]](#).
- [58] M. Döring, H. W. Hammer, M. Mai, J. Y. Pang, § A. Rusetsky, and J. Wu, “Three-body spectrum in a finite volume: the role of cubic symmetry,” *Phys. Rev. D* **97**, 114508 (2018), [arXiv:1802.03362 \[hep-lat\]](#).
- [59] Maxim Mai, Bin Hu, Michael Doring, Alessandro Pilloni, and Adam Szczepaniak, “Three-body scattering in isobar ansatz,” *PoS Hadron2017*, 140 (2018).
- [60] M. Mai and M. Döring, “Three-body Unitarity in the Finite Volume,” *Eur. Phys. J. A* **53**, 240 (2017), [arXiv:1709.08222 \[hep-lat\]](#).
- [61] Peng Guo and Michael Döring, “Lattice model of heavy-light three-body system,” *Phys. Rev. D* **101**, 034501 (2020), [arXiv:1910.08624 \[hep-lat\]](#).
- [62] Peng Guo, Michael Döring, and Adam P. Szczepaniak, “Variational approach to  $N$ -body interactions in finite volume,” *Phys. Rev. D* **98**, 094502 (2018), [arXiv:1810.01261 \[hep-lat\]](#).
- [63] M. Mikhasenko *et al.* (JPAC), “Dalitz-plot decomposition for three-body decays,” *Phys. Rev. D* **101**, 034033 (2020), [arXiv:1910.04566 \[hep-ph\]](#).
- [64] M. Albaladejo, D. Winney, I. V. Danilkin, C. Fernández-Ramírez, V. Mathieu, M. Mikhasenko, A. Pilloni, J. A. Silva-Castro, and A. P. Szczepaniak (JPAC), “Khuri-Treiman equations for  $3\pi$  decays of particles with spin,”

- Phys. Rev. D **101**, 054018 (2020), arXiv:1910.03107 [hep-ph].
- [65] M. Mikhasenko, Y. Wunderlich, A. Jackura, V. Mathieu, A. Pilloni, B. Ketzer, and A. P. Szczepaniak, “Three-body scattering: Ladders and Resonances,” *JHEP* **08**, 080 (2019), arXiv:1904.11894 [hep-ph].
- [66] L. Ng, L. Bibrzycki, J. Nys, C. Fernandez-Ramirez, A. Pilloni, V. Mathieu, A. J. Rasmusson, and A. P. Szczepaniak (Joint Physics Analysis Center, JPAC), “Deep learning exotic hadrons,” *Phys. Rev. D* **105**, L091501 (2022), arXiv:2110.13742 [hep-ph].
- [67] L. Ng, L. Bibrzycki, J. Nys, C. Fernández-Ramírez, A. Pilloni, V. Mathieu, A. J. Rasmusson, and A. P. Szczepaniak, “Machine learning exotic hadrons,” *Nuovo Cim. C* **47**, 207 (2024).
- [68] Leonarc Michelle Santos, Vince Angelo A. Chavez, and Denny Lane B. Sombillo, “Pole structure of  $P\psi N(4312)+$  via machine learning and uniformized S-matrix,” *J. Phys. G* **52**, 015104 (2025), arXiv:2405.11906 [hep-ph].
- [69] Vince Angelo A. Chavez and Denny Lane B. Sombillo, “Line shape analysis of  $\Lambda(1405)$  in  $\gamma p \rightarrow K^+\Sigma^-\pi^+$  reaction using convolutional neural network,” in *21st International Conference on Hadron Spectroscopy and Structure* (2025) arXiv:2506.04622 [hep-ph].
- [70] M. Malekhsosini, S. Rostami, A. R. Olamaei, R. Ostovar, and K. Azizi, “Meson mass and width: Deep learning approach,” *Phys. Rev. D* **110**, 054011 (2024), arXiv:2404.00448 [hep-ph].
- [71] Darwin Alexander O. Co and Denny Lane B. Sombillo, “Analysis of hidden-charm pentaquarks as triangle singularities via deep learning,” *PoS QNP2024*, 031 (2025), arXiv:2411.14044 [hep-ph].
- [72] Aurélien Dersy, Matthew D. Schwartz, and Alexander Zhiboedov, “Reconstructing S-matrix Phases with Machine Learning,” *JHEP* **05**, 200 (2024), arXiv:2308.09451 [hep-th].
- [73] Adam B. Mapa and Denny Lane B. Sombillo, “Feature extraction in partial wave analysis using  $K$ -matrix approach,” in *21st International Conference on Hadron Spectroscopy and Structure* (2025) arXiv:2506.04628 [hep-ph].
- [74] Darwin Alexander O. Co, Vince Angelo A. Chavez, and Denny Lane B. Sombillo, “Deep learning framework for disentangling triangle singularity and pole-based enhancements,” *Phys. Rev. D* **110**, 114034 (2024), arXiv:2403.18265 [hep-ph].
- [75] Denny Lane Sombillo, “Extraction of S-matrix pole structure using deep learning,” *PoS PANIC2021*, 175 (2022).
- [76] Denny Lane B. Sombillo, Yoichi Ikeda, Toru Sato, and Atsushi Hosaka, “Classifying Near-Threshold Enhancement Using Deep Neural Network,” *Few Body Syst.* **62**, 52 (2021), arXiv:2106.03453 [hep-ph].
- [77] Denny Lane B. Sombillo, Yoichi Ikeda, Toru Sato, and Atsushi Hosaka, “Model independent analysis of coupled-channel scattering: A deep learning approach,” *Phys. Rev. D* **104**, 036001 (2021), arXiv:2105.04898 [hep-ph].
- [78] Denny Lane B. Sombillo, Yoichi Ikeda, Toru Sato, and Atsushi Hosaka, “Unveiling the pole structure of S-matrix using deep learning,” *Rev. Mex. Fis. Suppl.* **3**, 0308067 (2022), arXiv:2104.14182 [hep-ph].
- [79] Denny Lane B. Sombillo, Yoichi Ikeda, Toru Sato, and Atsushi Hosaka, “Classifying the pole of an amplitude using a deep neural network,” *Phys. Rev. D* **102**, 016024 (2020), arXiv:2003.10770 [hep-ph].
- [80] J. Landay, M. Mai, M. Döring, H. Habermann, and K. Nakayama, “Towards the Minimal Spectrum of Excited Baryons,” *Phys. Rev. D* **99**, 016001 (2019), arXiv:1810.00075 [nucl-th].
- [81] R. Molina, Justin Landay, Bin Hu, Michael Doring, and Cesar Fernández-Ramírez, “Model selection for pion photoproduction,” *PoS Hadron2017*, 135 (2018).
- [82] Dimitrios Petrellis and Dalibor Skoupil, “Ridge regression for minimizing the couplings of hyperon resonances in  $K+\Lambda$  photoproduction,” *Phys. Rev. C* **107**, 045206 (2023), arXiv:2212.14305 [nucl-th].
- [83] Petr Bydžovský, Aleš Cieplý, Dimitrios Petrellis, Dalibor Skoupil, and Nicholas Zachariou, “Model selection for  $K+\Sigma^-$  photoproduction within an isobar model,” *Phys. Rev. C* **104**, 065202 (2021), [Erratum: Phys.Rev.C 110, 029901 (2024)], arXiv:2106.15199 [nucl-th].
- [84] T. Alghamdi *et al.*, “Toward a generative modeling analysis of CLAS exclusive  $2\pi$  photoproduction,” *Phys. Rev. D* **108**, 094030 (2023), arXiv:2307.04450 [hep-ph].
- [85] Daniele Binosi, Alessandro Pilloni, and Ralf-Arno Tripolt, “Study for a model-independent pole determination of overlapping resonances,” *Phys. Lett. B* **839**, 137809 (2023), arXiv:2205.02690 [hep-ph].
- [86] Daniel Sadasivan, Maxim Mai, Michael Döring, Ulf-G. Meißner, Felipe Amorim, John Paul Klucik, Jun-Xu Lu, and Li-Sheng Geng, “New insights into the pole parameters of the  $\Lambda(1380)$ , the  $\Lambda(1405)$  and the  $\Sigma(1385)$ ,” *Front. Phys.* **11**, 1139236 (2023), arXiv:2212.10415 [nucl-th].
- [87] Feng-Kun Guo, Yuki Kamiya, Maxim Mai, and Ulf-G. Meißner, “New insights into the nature of the  $\Lambda(1380)$  and  $\Lambda(1405)$  resonances away from the SU(3) limit,” *Phys. Lett. B* **846**, 138264 (2023), arXiv:2308.07658 [hep-ph].
- [88] P. C. Bruns, A. Cieplý, and M. Mai, “Testing chiral unitary models for the  $\Lambda(1405)$  in  $K+\pi\Sigma$  photoproduction,” *Phys. Rev. D* **106**, 074017 (2022).
- [89] Maxim Mai, “Status of the  $\Lambda(1405)$ ,” *Few Body Syst.* **59**, 61 (2018).
- [90] Ales Cieplý and Maxim Mai, “Theoretical approaches to low energy  $\bar{K}N$  interactions,” *EPJ Web Conf.* **130**, 02001 (2016), arXiv:1610.06444 [nucl-th].
- [91] A. Cieplý, M. Mai, Ulf-G. Meißner, and J. Smejkal, “On the pole content of coupled channels chiral approaches used for the  $\bar{K}N$  system,” *Nucl. Phys. A* **954**, 17–40 (2016), arXiv:1603.02531 [hep-ph].
- [92] Maxim Mai and Ulf-G. Meißner, “Constraints on the chiral unitary  $\bar{K}N$  amplitude from  $\pi\Sigma K^+$  photoproduction data,” *Eur. Phys. J. A* **51**, 30 (2015), arXiv:1411.7884 [hep-ph].
- [93] Albert Feijoo, Volodymyr Magas, and Angels Ramos, “ $S=-1$  meson-baryon interaction and the role of isospin filtering processes,” *Phys. Rev. C* **99**, 035211 (2019), arXiv:1810.07600 [hep-ph].
- [94] S. Navas *et al.* (Particle Data Group), “Review of particle physics,” *Phys. Rev. D* **110**, 030001 (2024).
- [95] Martin Hoferichter, Jacobo Ruiz de Elvira, Bastian Kubis, and Ulf-G. Meißner, “Nucleon resonance parameters from Roy–Steiner equations,” *Phys. Lett. B* **853**, 138698 (2024), arXiv:2312.15015 [hep-ph].
- [96] R. Garcia-Martin, R. Kaminski, J. R. Pelaez, and J. Ruiz de Elvira, “Precise determination of the  $f_0(600)$  and  $f_0(980)$  pole parameters from a dispersive

- data analysis,” *Phys. Rev. Lett.* **107**, 072001 (2011), [arXiv:1107.1635 \[hep-ph\]](#).
- [97] J. R. Pelaez, “Light scalars as tetraquarks or two-meson states from large  $N(c)$  and unitarized chiral perturbation theory,” *Mod. Phys. Lett. A* **19**, 2879–2894 (2004), [arXiv:hep-ph/0411107](#).
- [98] Joel Grus, *Data Science from Scratch: First Principles with Python*, 2nd ed. (O’Reilly Media, Sebastopol, CA, 2019).